LETTER

doi:10.1038/nature12397

Changes in North Atlantic nitrogen fixation controlled by ocean circulation

Marietta Straub[1], Daniel M. Sigman[2], Haojia Ren[3], Alfredo Martínez-García[1], A. Nele Meckler[1], Mathis P. Hain[2] & Gerald H. Haug[1]

In the ocean, the chemical forms of nitrogen that are readily available for biological use (known collectively as 'fixed' nitrogen) fuel the global phytoplankton productivity that exports carbon to the deep ocean[1–3]. Accordingly, variation in the oceanic fixed nitrogen reservoir has been proposed as a cause of glacial–interglacial changes in atmospheric carbon dioxide concentration[2,3]. Marine nitrogen fixation, which produces most of the ocean's fixed nitrogen, is thought to be affected by multiple factors, including ocean temperature[4] and the availability of iron[2,3,5] and phosphorus[6]. Here we reconstruct changes in North Atlantic nitrogen fixation over the past 160,000 years from the shell-bound nitrogen isotope ratio ($^{15}N/^{14}N$) of planktonic foraminifera in Caribbean Sea sediments. The observed changes cannot be explained by reconstructed changes in temperature, the supply of (iron-bearing) dust or water column denitrification. We identify a strong, roughly 23,000-year cycle in nitrogen fixation and suggest that it is a response to orbitally driven changes in equatorial Atlantic upwelling[7], which imports 'excess' phosphorus (phosphorus in stoichiometric excess of fixed nitrogen) into the tropical North Atlantic surface[5,6]. In addition, we find that nitrogen fixation was reduced during glacial stages 6 and 4, when North Atlantic Deep Water had shoaled to become glacial North Atlantic intermediate water[8], which isolated the Atlantic thermocline from excess phosphorus-rich mid-depth waters that today enter from the Southern Ocean. Although modern studies have yielded diverse views of the controls on nitrogen fixation[1,2,4,5], our palaeobiogeochemical data suggest that excess phosphorus is the master variable in the North Atlantic Ocean and indicate that the variations in its supply over the most recent glacial cycle were dominated by the response of regional ocean circulation to the orbital cycles.

Nitrogen fixation, the conversion of N_2 to ammonia, by cyanobacteria in surface waters seems to dominate the input of fixed N to the ocean. The main loss of fixed N is biological reduction to N_2 (generalized here as 'denitrification') in marine sediments and in the suboxic zones of the water column in the eastern tropical Pacific Ocean and the Arabian Sea[1]. Nitrogen fixation introduces N with $\delta^{15}N$ of about −1‰ ($\delta^{15}N = (^{15}N/^{14}N)_{sample}/(^{15}N/^{14}N)_{reference} - 1$, where the reference is atmospheric N_2), whereas water column denitrification preferentially removes ^{14}N-bearing nitrate[9] (NO_3^-). In total, global ocean denitrification raises the $\delta^{15}N$ of mean ocean nitrate above that of newly fixed N (ref. 10).

Sediment records show N isotopic evidence of reduced water column denitrification during the Last Glacial Maximum (LGM) and other cold phases of the most recent glacial cycle, relative to the current interglacial (the Holocene epoch) and times of intermediate climate states[11] (for example Marine Isotope Stage (MIS) 3, from 57 to 29 kyr ago). Benthic denitrification, because of its weak effect on the $\delta^{15}N$ value of nitrate in the water column[10], has not been directly reconstructed, but it may also have decreased during ice ages because of reduced continental shelf area due to lower sea level[12].

The history of N fixation has been vigorously debated[2,3,13]. As with water column denitrification, N fixation is apparent in the spatial pattern of nitrate $\delta^{15}N$. Against the background of the mean ocean nitrate $\delta^{15}N$ of ~5‰, N fixation in the euphotic zone followed by the sinking and remineralization of organic matter adds low-$\delta^{15}N$ nitrate to the thermocline, which is observed across the western subtropical and tropical North Atlantic[14]. This low $\delta^{15}N$ value is recorded by the organic N bound within the shell walls of planktonic foraminifera[15,16]. Foraminifera-bound $\delta^{15}N$ (FB-$\delta^{15}N$) from the Caribbean Sea and the Gulf of Mexico indicates that N fixation was reduced during the LGM[15,17].

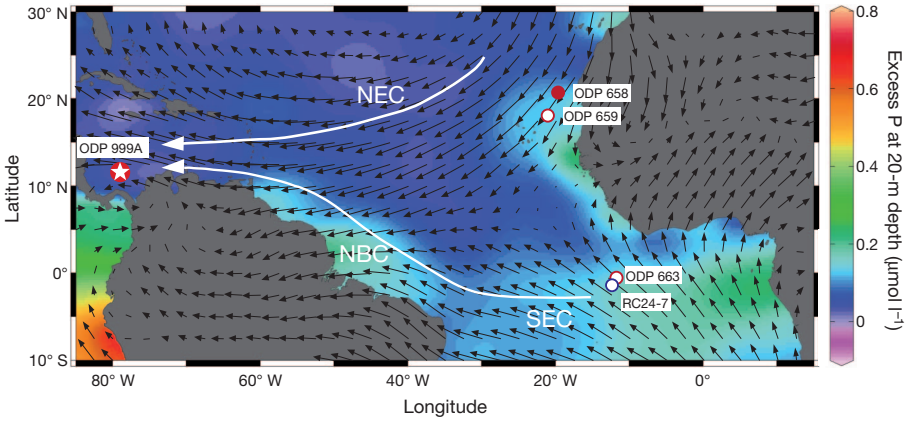

Figure 1 | Core locations, surface winds, excess P at 20-m depth and main surface currents. The star indicates ODP Site 999 Hole A (12° 45′ N, 78° 44′ W; 2,828 m), the core in which FB-$\delta^{15}N$ was measured to reconstruct North Atlantic N fixation. The filled red circle indicates ODP Site 658 (20° 45′ N, 18° 35′ W; 2,263 m), from which sediment Zr/Al data are reported in relation to North African aeolian flux. The open blue circle indicates core RC24-7 (1° 21′ S, 11° 55′ W; 3,899 m), previously published data from which reveal precession cycles in equatorial Atlantic upwelling[7]. The open red circles indicate ODP Site 659 (18° 05′ N, 21° 02′ W; 3,070 m) and ODP Site 663 (1° 11.9′ S, 11° 52.7′ W; 3,708 m), from which come previously published data pertaining to the aeolian flux[21,22]. Excess P ($[PO_4^{3-}] - [NO_3^-]/16$; ref. 6) is an annual average. Black arrows show June–August winds, with length indicating speed. NBC, north Brazil current; NEC, north equatorial current; SEC, south equatorial current.

[1]Geological Institute, Department of Earth Sciences, ETH Zurich, 8092 Zurich, Switzerland. [2]Department of Geosciences, Princeton University, Princeton, New Jersey 08544, USA. [3]Lamont-Doherty Earth Observatory, Columbia University, New York, New York 10964, USA.

Here we build on the FB-δ^{15}N results of ref. 15 with new data from the same core, Ocean Drilling Program (ODP) Site 999 Hole A in the Caribbean Sea (Fig. 1), extending the record back over the past 160 kyr through a full glacial cycle (Fig. 2a, b). We measured FB-δ^{15}N in two euphotic-zone-dwelling species of planktonic foraminifera, *Globigerinoides ruber* and *Globigerinoides sacculifer*. The records from the two species are very similar (Fig. 2a and Supplementary Fig. 1) and highly coherent (Supplementary Fig. 6). The FB-δ^{15}N of *G. ruber* (Fig. 2a, green symbols) is typically slightly (~0.3‰) lower than that of *G. sacculifer* (Fig. 2a, blue symbols). There is a greater (≥0.6‰) interspecies difference during the LGM, in glacial MIS 4 and during the transition from MIS 6 to MIS 5 (Fig. 2a and Supplementary Fig. 1). Although changes in the interspecies

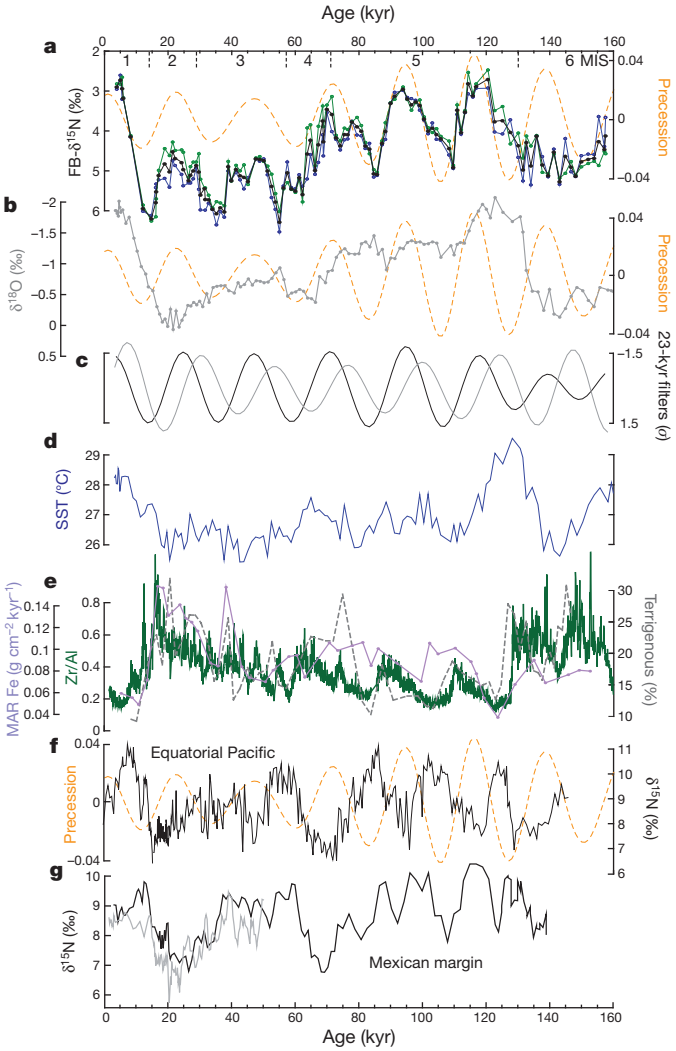

Figure 2 | FB-δ^{15}N in ODP Site 999 and its relationship to SST, dust flux and water column denitrification. a, FB-δ^{15}N was measured separately in two species, *G. sacculifer* (blue) and *G. ruber* (green). The black symbols show the two-species average FB-δ^{15}N at each sampling depth. As plotted, increasing N fixation is upward. **b**, *Globigerinoides ruber* δ^{18}O at ODP Site 999[20]. In **a** and **b**, precession is dashed orange. **c**, The 23-kyr precession-band-filtered FB-δ^{15}N (black) and *G. ruber* δ^{18}O (grey) illustrate the 4–7-kyr phase lag between δ^{15}N and δ^{18}O at the precession band (Supplementary Figs 6 and 9). Given an average phase lag of 4–7 kyr between δ^{18}O and precession[19], this observation confirms the correspondence of δ^{15}N minima with precession maxima (June aphelion). ($\delta^{18}O = (^{18}O/^{16}O)_{sample}/(^{18}O/^{16}O)_{reference} - 1$, where the reference is Vienna PeeDee Belemnite.) **d**, *Globigerinoides ruber* Mg/Ca-derived SST at ODP Site 999[20]. **e**, Atlantic dust-related records are mass accumulation rate of iron (MAR Fe) at ODP Site 999[23], Zr/Al at ODP Site 658 and terrigenous material abundance at ODP Site 663[22]. **f**, **g**, The Pacific bulk sediment δ^{15}N records are from the Mexican margin[29] (**g**) and the equatorial Pacific[30] (**f**), with increasing denitrification plotted upward (see also Supplementary Fig. 5).

δ^{15}N difference probably hold valuable information[16], given the overarching similarity of the *G. ruber* and *G. sacculifer* FB-δ^{15}N records, we focus hereafter on the FB-δ^{15}N record generated by averaging the two species-specific records (Fig. 2a, black symbols).

The FB-δ^{15}N of the previous interglacial (early MIS 5) is similar to that of the Holocene, and the FB-δ^{15}N of the penultimate glacial maximum (MIS 6) is similar to that of the LGM. There is no evidence from previous work for mean ocean nitrate δ^{15}N changes across the most recent glacial cycle that mimic the FB-δ^{15}N record of Site 999, with the exception of a possible δ^{15}N maximum during the most recent deglaciation[15,18]. Furthermore, South China Sea FB-δ^{15}N data support the interpretation of the Caribbean LGM-to-Holocene FB-δ^{15}N decrease as recording a regional change in N fixation[18]. The FB-δ^{15}N change through the Caribbean Sea record is of similar amplitude to the regional isotopic imprint of N fixation, in which nitrate δ^{15}N decreases from ~5.3‰ at ~1,200-m depth in the water column to ~2.5‰ at ~200 m (ref. 14). Thus, the FB-δ^{15}N record indicates proportionally large variations in N fixation[15]. The record of bulk sediment δ^{15}N at Site 999 shows a number of minor changes that coincide with changes in FB-δ^{15}N, but they are so weak as to be unnoticeable without the benefit of the larger FB-δ^{15}N changes (Supplementary Fig. 2). The apparent muting of the variations suggests an allochthonous N input to the bulk sediment that does not respond to open-ocean changes[17].

The FB-δ^{15}N variation is highly correlated with Earth's 19–23-kyr orbital precession cycle (Fig. 2a and Supplementary Figs 6, 8 and 10). FB-δ^{15}N minima consistently lag *G. ruber* calcite δ^{18}O minima by 4–7 kyr (Fig. 2c and Supplementary Figs 6 and 9), and they thus lag peak Northern Hemisphere summer insolation at the precession frequency band by 10–12 kyr (ref. 19). That is, minima in Caribbean FB-δ^{15}N (maxima in N fixation) occur during aphelion in the northern summer (precession maxima; Fig. 2a), which is the opposite of the precession phase that encourages Northern Hemisphere summer warming and deglaciation. Despite this precessional phasing, FB-δ^{15}N is higher (N fixation is reduced) during the major glacial periods (MIS 6 and MISs 4–2) relative to the interglacials (MISs 5 and 1). This implies that there are non-precessional step changes in FB-δ^{15}N at each of the major deglaciations (the transitions between MISs 6 and 5 and between MISs 2 and 1) and at the intensification of glaciation at the transition between MISs 5 and 4.

Temperature is recognized as a control on the distribution of N fixation, both in the ocean and on land[4]. Thus, ice-age cooling might be expected to reduce N fixation, consistent with the basic LGM–Holocene change in N fixation. However, the full record indicates that N fixation does not track Caribbean sea surface temperature (SST) as reconstructed from the Mg/Ca ratio of *G. ruber* at Site 999[20] (Fig. 2d and Supplementary Fig. 9c). SST rose early in the penultimate deglaciation (the transition between MISs 6 and 5) and had already begun to decline before N fixation reached the first of its three maxima in MIS 5, with the subsequent maxima in N fixation occurring against a relatively stable baseline of low SST (Fig. 2d and Supplementary Fig. 7a, b). Hence, SST change does not seem to explain the history of N fixation reconstructed from FB-δ^{15}N.

Iron is a critical nutrient for N fixers, and iron-bearing dust has been suggested to cause ice-age enhancements in N fixation[2,3]. In our comparison of the N fixation record at Site 999 with records of dust input, we include a new reconstruction of dust transport from ODP Site 658, a coring site off the coast of North Africa, which is the dominant source of dust to the Caribbean (Fig. 1). The Zr/Al ratio increases with high-energy aeolian transport (Supplementary Fig. 3). Focusing first on the large-scale glacial–interglacial changes, the FB-δ^{15}N record at Site 999 indicates that N fixation was, if anything, inversely correlated with Zr/Al at Site 658; reconstructed dust flux at Site 659[21], which is farther offshore; terrigenous material abundance at equatorial Atlantic Site 663[22]; and iron accumulation rate at Site 999[23] (Fig. 2e and Supplementary Fig. 4). The correlation of N fixation with dust over the precession cycle is more difficult to assess. North African aridity has

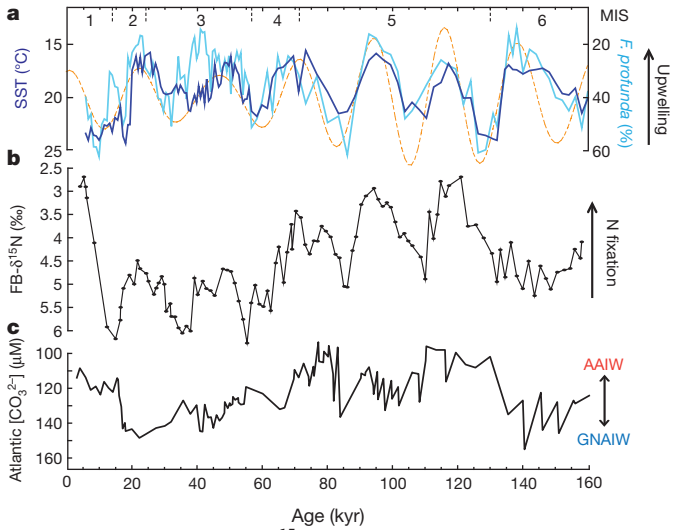

Figure 3 | Comparison of FB-δ^{15}N with changes in precession-paced equatorial Atlantic upwelling and glacial–interglacial Atlantic intermediate water source. **a**, *Florisphaera profunda* abundance (light blue) and foraminifera-species-derived SST (dark blue) from equatorial Atlantic core RC24-7[7]. **b**, FB-δ^{15}N from ODP Site 999. **c**, Bottom water carbonate ion reconstruction from Caribbean Sea core VM28-122[31] (12° N, 79° W; 3,620 m). The orange dashed line in **a** is the precession parameter. Episodes of higher equatorial Atlantic upwelling led to higher N fixation in the North Atlantic, observed as lower FB-δ^{15}N. In **c**, the switches in North Atlantic intermediate water source between AAIW, the dominant source of excess P to the Atlantic[5], and GNAIW, which was low in [PO_4^{3-}] (refs 28,32) and presumably also in excess P, can be seen. Periods of inflow of AAIW stimulated N fixation.

been reported to increase during northern summer aphelion[24], when we observe higher N fixation. However, available records suggest, on balance, that dust input is out of phase with the precessional cycles in N fixation (Fig. 2 and Supplementary Information). All things considered, it does not seem that a dust-derived iron supply can explain the reconstructed N fixation changes.

North Atlantic N fixation might be expected to change so as to balance denitrification changes[13]. Bulk sediment δ^{15}N records near the major suboxic zones indicate a lower rate of water column denitrification during cold periods[11], in the same sense as the N fixation decrease that we reconstruct for the LGM, the glacial of MIS 4 and the glacial maximum of MIS 6 (Fig. 2f, g and Supplementary Fig. 5). However, beyond this coarsest scale, there are major differences. For example, in contrast to the sediment δ^{15}N records from the denitrification zones, FB-δ^{15}N at Site 999 during early MIS 3 is similar to that during the LGM, with these local δ^{15}N minima separated by the highest sustained δ^{15}N of the record at ~35 kyr ago in late MIS 3 (Fig. 2a). In addition, tropical Pacific bulk sediment δ^{15}N maxima (water column denitrification maxima) seem to be associated with minima in Earth's orbital precession cycle (Fig. 2f), when perihelion coincides with northern summer. The FB-δ^{15}N record indicates that these times represent minima, not maxima, in Atlantic N fixation. Although a global ocean reconstruction of denitrification does not yet exist, the available records do not provide clear signs that changes in water column denitrification are responsible for the timing of changes in North Atlantic N fixation over the most recent glacial cycle.

The importance of precession in Caribbean FB-δ^{15}N suggests a connection to low-latitude climate. Over recent glacial cycles, equatorial Atlantic upwelling varied with a precession frequency[7]. In the eastern equatorial Atlantic, climatic precession maxima (aphelion in northern summer) coincide with minima in reconstructed SST (Fig. 3a). In addition, these times are characterized by minima in the fraction of the nanofossils represented by the nutricline dwelling form *Florisphaera profunda* (Fig. 3a), reflecting a shoaling of the nutricline[7]. These observations indicate that precession maxima yielded stronger equatorial Atlantic upwelling[7].

Precession-paced change in the equatorial Atlantic upwelling, coupled with a tendency of N fixation to occur in N-depleted, phosphorus-bearing water[6], explains the precession signal in Caribbean FB-δ^{15}N. Compared with the thermocline and surface layer of the western North Atlantic, subsurface water upwelled along the Equator has higher 'excess P'[5,6] (defined as the phosphate concentration minus 1/16th of the nitrate concentration; Fig. 1). In waters with positive excess P, phytoplankton tends to deplete the water of nitrate before the complete consumption of phosphate. The residual phosphate in this nitrate-free water should encourage the growth of N-fixing phytoplankton[13]. In line with this expectation, data-assimilating model calculations suggest that the transport into the tropical North Atlantic of equatorial water bearing excess P leads to a band of high N fixation in this region[6,25]. Moreover, N fixation seems to respond in the equatorial Atlantic upwelling region itself, before lateral transport of surface waters[26]. The excess P of the waters upwelled along the Equator originates in sub-Antarctic mode water (SAMW) and Antarctic intermediate water[5] (AAIW). With climatic precession maxima, increased equatorial upwelling of excess-P-bearing water coupled with northwestward transport of equatorial surface waters into the western tropical North Atlantic by the north Brazil current would increase the supply of excess P to the latter region, intensifying N fixation there (Fig. 3). Although the Amazon outflow may also contribute to the excess P in the north Brazil current (Fig. 1), its response to precession[27] seems to be inconsistent with our reconstructed N fixation changes.

The baseline shifts in FB-δ^{15}N at the respective transitions between MISs 6 and 5, 5 and 4, and 2 and 1 parallel well-known changes in the depth of North Atlantic ventilation (Fig. 3c): glacial North Atlantic intermediate water (GNAIW) formed during glacial stages 6 and 4–2, rather than the North Atlantic Deep Water (NADW) of interglacial stages[8]. GNAIW formation reduced the nutrient concentration at the base of the Atlantic thermocline[28] by preventing the influx of AAIW and SAMW or by diluting their impact, or both (Fig. 4). The low nutrient content of GNAIW implies that it formed from nutrient-depleted, low-latitude North Atlantic surface water, which today lacks excess P (ref. 5). Thus, the switch from NADW to GNAIW lowered the excess P of the subsurface waters to be upwelled (Fig. 4). A plausible alternative for the step changes in FB-δ^{15}N is that Atlantic N fixation was responding to sea-level-driven reductions in sedimentary denitrification during glacial stages 6 and 4–2. However, a shelf-associated decrease in sedimentary denitrification would have lowered excess P in the low-latitude upper ocean within decades to centuries of the sea-level decline at the onset of MIS 4. The FB-δ^{15}N increase in glacial stage 4 occurred ~7 kyr after the sea-level decrease (Fig. 2a, b and Supplementary Fig. 9a), inconsistent with a response to regional sedimentary denitrification but consistent with the timing of the switch to GNAIW[8].

Although variations in Atlantic N fixation do not seem to have paralleled global water column denitrification over the past 160 kyr, this does not require an imbalance between N fixation and denitrification on a global ocean basis; indeed, a sensitivity to phosphorus would encourage a global balance[13]. At the same time, this study recalibrates our expectations regarding the regional drivers of biogeochemical change in the low-nutrient tropical and subtropical ocean. Water column denitrification is broadly recognized as being sensitive to the physical circulation, given that the major ocean suboxic regions are located in the tropical 'shadow zones', the poorly ventilated subsurface volumes east of the subtropical gyres. Our results indicate that ocean circulation, through its control of nutrient transport, can also drive changes in regional rates of N fixation[6].

Although iron limitation of phytoplankton is fundamental to ocean biogeochemistry[2,3,5], the data reported here suggest that, in the North Atlantic, the rate of N fixation over the past 160 kyr has not been tightly constrained by iron supply. The entire ocean N and P reservoirs must flow through the North Atlantic on the timescale of ocean ventilation (~1 kyr), which is probably shorter than the residence time of the ocean's fixed N reservoir[1]. Thus, if N fixation in the rest of the ocean is significantly limited

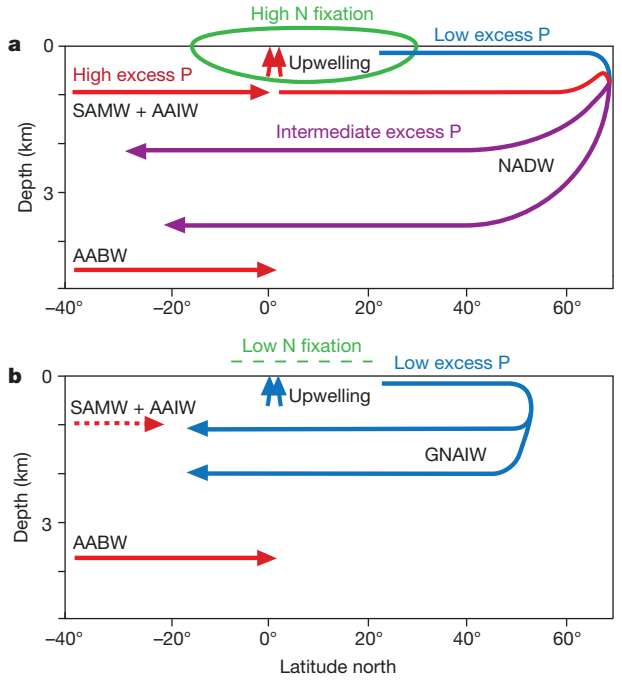

Figure 4 | Effect of changes in glacial–interglacial circulation on N fixation in the Atlantic. a, During the Holocene and MIS 5, SAMW and AAIW import high excess P (red) to the low latitudes, where its upwelling stimulates N fixation, which removes the excess P (conversion from red to blue). North Atlantic surface water, SAMW and AAIW are incorporated into newly formed NADW, which is thus intermediate in excess P (purple; ref. 5). **b**, In glacial stages MIS 6 and MISs 4–2 (where MIS 2 is the LGM), the low excess P of southward-flowing GNAIW would have diluted or replaced the high excess P of SAMW and AAIW, reducing the concentration of excess P available to be upwelled, and thus lowering N fixation. The precession-paced changes in equatorial Atlantic upwelling are not indicated in this diagram.

by iron, then the North Atlantic may have an important role in maintaining the relationship between the global ocean N and P reservoirs.

METHODS SUMMARY

FB-δ^{15}N was analysed by oxidizing organic N to nitrate and then using a bacterial method to convert the nitrate to nitrous oxide for isotope ratio mass spectrometry[15]. The individual species were picked manually, to obtain 3–7 mg of foraminifera per sample. The picked sample was crushed and underwent reductive and then oxidative cleaning to remove all N not bound within (and thus physically protected by) the calcite walls of the foraminifera tests. Dissolution of the tests with HCl released the test-bound organic N, which was then oxidized to nitrate. Sediment Zr/Al was measured with an Avaatech XRF Core Scanner at MARUM, University of Bremen. Data are of X-ray fluorescence count ratios and were obtained at a resolution of 1 cm over an area of 1.2 cm^2 directly at the split-core surface of the archive half.

Full Methods and any associated references are available in the online version of the paper.

Received 22 August 2012; accepted 13 June 2013.
Published online 21 August 2013.

1. Gruber, N. & Galloway, J. N. An Earth-system perspective of the global nitrogen cycle. *Nature* **451,** 293–296 (2008).
2. Falkowski, P. G. Evolution of the nitrogen cycle and its influence on the biological sequestration of CO_2 in the ocean. *Nature* **387,** 272–275 (1997).
3. Broecker, W. S. & Henderson, G. M. The sequence of events surrounding Termination II and their implications for the cause of glacial-interglacial CO_2 changes. *Paleoceanography* **13,** 352–364 (1998).
4. Houlton, B. Z., Wang, Y., Vitousek, P. M. & Field, C. B. A unifying framework for dinitrogen fixation in the terrestrial biosphere. *Nature* **454,** 327–330 (2008).
5. Moore, C. M. *et al.* Large-scale distribution of Atlantic nitrogen fixation controlled by iron availability. *Nature Geosci.* **2,** 867–871 (2009).
6. Deutsch, C., Sarmiento, J. L., Sigman, D. M., Gruber, N. & Dunne, J. P. Spatial coupling of nitrogen inputs and losses in the ocean. *Nature* **445,** 163–167 (2007).
7. Molfino, B. & McIntyre, A. Precessional forcing of nutricline dynamics in the equatorial Atlantic. *Science* **249,** 766–769 (1990).
8. Piotrowski, A. M., Goldstein, S. L., Hemming, S. R. & Fairbanks, R. G. Temporal relationships of carbon cycling and ocean circulation at glacial boundaries. *Science* **307,** 1933–1938 (2005).
9. Brandes, J. A., Devol, A. H., Yoshinari, T., Jayakumar, D. A. & Naqvi, S. W. A. Isotopic composition of nitrate in the central Arabian Sea and eastern tropical North Pacific: a tracer for mixing and nitrogen cycles. *Limnol. Oceanogr.* **43,** 1680–1689 (1998).
10. Brandes, J. A. & Devol, A. H. A global marine-fixed nitrogen isotopic budget: implications for Holocene nitrogen cycling. *Glob. Biogeochem. Cycles* **16,** 1120 (2002).
11. Altabet, M. A., Francois, R., Murray, D. W. & Prell, W. L. Climate-related variations in denitrification in the Arabian Sea from sediment $^{15}N/^{14}N$ ratios. *Nature* **373,** 506–509 (1995).
12. Christensen, J. P. Carbon export from continental shelves, denitrification and atmospheric carbon dioxide. *Cont. Shelf Res.* **14,** 547–576 (1994).
13. Tyrrell, T. The relative influences of nitrogen and phosphorus on oceanic primary production. *Nature* **400,** 525–531 (1999).
14. Knapp, A. N., DiFiore, P. J., Deutsch, C., Sigman, D. M. & Lipschultz, F. Nitrate isotopic composition between Bermuda and Puerto Rico: implications for N_2 fixation in the Atlantic Ocean. *Glob. Biogeochem. Cycles* **22,** GB3014 (2008).
15. Ren, H. *et al.* Foraminiferal isotope evidence of reduced nitrogen fixation in the ice age Atlantic Ocean. *Science* **323,** 244–248 (2009).
16. Ren, H., Sigman, D. M., Thunell, R. C. & Prokopenko, M. G. Nitrogen isotopic composition of planktonic foraminifera from the modern ocean and recent sediments. *Limnol. Oceanogr.* **57,** 1011–1024 (2012).
17. Meckler, A. N. *et al.* Deglacial nitrogen isotope changes in the Gulf of Mexico: evidence from bulk sedimentary and foraminifera-bound nitrogen in Orca Basin sediments. *Paleoceanography* **26,** PA4216 (2011).
18. Ren, H., Sigman, D. M., Chen, M. C. & Kao, S. Elevated foraminifera-bound nitrogen isotopic composition during the last ice age in the South China Sea and its global and regional implications. *Glob. Biogeochem. Cycles* **26,** GB1031 (2012).
19. Imbrie, J. *et al.* On the structure and origin of major glaciation cycles 1. Linear responses to Milankovitch forcing. *Paleoceanography* **7,** 701–738 (1992).
20. Schmidt, M. W., Vautravers, M. J. & Spero, H. J. Western Caribbean sea surface temperatures during the late Quaternary. *Geochem. Geophys. Geosyst.* **7,** Q02P10 (2006).
21. Tiedemann, R., Sarnthein, M. & Shackleton, N. J. Astronomic timescale for the Pliocene Atlantic $\delta^{18}O$ and dust flux records of Ocean Drilling Program site 659. *Paleoceanography* **9,** 619–638 (1994).
22. deMenocal, P. B., Ruddiman, W. F. & Pokras, E. M. Influences of high- and low-latitude processes on African terrestrial climate: Pleistocene eolian records from equatorial Atlantic Ocean Drilling Program Site 663. *Paleoceanography* **8,** 209–242 (1993).
23. Mora, G. & Martínez, J. I. Sedimentary metal ratios in the Colombia Basin as indicators for water balance change in northern South America during the past 400,000 years. *Paleoceanography* **20,** PA4013 (2005).
24. Pokras, E. M. & Mix, A. C. Earth's precession cycle and Quaternary climatic change in tropical Africa. *Nature* **326,** 486–487 (1987).
25. Coles, V. J. & Hood, R. R. Modeling the impact of iron and phosphorus limitations on nitrogen fixation in the Atlantic Ocean. *Biogeosciences* **4,** 455–479 (2007).
26. Subramaniam, A., Mahaffey, C., Johns, W. & Mahowald, N. Equatorial upwelling enhances nitrogen fixation in the Atlantic Ocean. *Geophys. Res. Lett.* **40,** 1766–1771 (2013).
27. Harris, S. E. & Mix, A. C. Pleistocene precipitation balance in the Amazon basin recorded in deep sea sediments. *Quat. Res.* **51,** 14–26 (1999).
28. Marchitto, T. M., Curry, W. B. & Oppo, D. W. Millennial-scale changes in North Atlantic circulation since the last glaciation. *Nature* **393,** 557–561 (1998).
29. Ganeshram, R. S., Pedersen, T. F., Calvert, S. E. & Murray, D. W. Large changes in oceanic nutrient inventories from glacial to interglacial periods. *Nature* **376,** 755–758 (1995).
30. Jia, G. & Li, Z. Easterly denitrification signal and nitrogen fixation feedback documented in the western Pacific sediments. *Geophys. Res. Lett.* **38,** L24605 (2011).
31. Yu, J. *et al.* An evaluation of benthic foraminiferal B/Ca and $\delta^{11}B$ for deep ocean carbonate ion and pH reconstructions. *Earth Planet. Sci. Lett.* **293,** 114–120 (2010).
32. Marchitto, T. M. & Broecker, W. S. Deep water mass geometry in the glacial Atlantic Ocean: a review of constraints from the paleonutrient proxy Cd/Ca. *Geochem. Geophys. Geosyst.* **7,** Q12003 (2006).

Supplementary Information is available in the online version of the paper.

Acknowledgements We thank M. A. Weigand, S. Oleynik and S. Bishop for technical assistance and U. Röhl and V. Lukies for X-ray fluorescence scanning support. Funding was from SNF grant 200021-131886/1, US NSF grant OCE-1060947 and the Grand Challenges Program of Princeton University. This research used samples provided by the ODP, which is sponsored by the NSF and participating countries under the management of the Joint Oceanographic Institutions. X-ray fluorescence scanning was supported by the DFG-Leibniz Center for Surface Process and Climate Studies at the University of Potsdam.

Author Contributions M.S., D.M.S. and G.H.H. designed the study. M.S. performed the FB-δ^{15}N analysis and wrote the first version of the manuscript with D.M.S.; A.N.M. generated the Zr/Al record at ODP Site 658. A.M.-G. performed the statistical analysis of the data with M.S.; H.R. was involved in the laboratory and data analysis. All authors contributed to the interpretation of the data and provided significant input to the final manuscript.

Author Information Reprints and permissions information is available at www.nature.com/reprints. The authors declare no competing financial interests. Readers are welcome to comment on the online version of the paper. Correspondence and requests for materials should be addressed to M.S. (marietta.straub@alumni.ethz.ch).

METHODS

Sample preparation for FB-δ^{15}N. The protocol follows that of ref. 15. The individual species are picked manually under a dissecting microscope (315–425-μm size fraction). Foraminifera (3–7 mg, or 600–800 specimens, per sample) are used to carry out the analysis and are gently crushed. Clay particles are removed using a 2% polyphosphate solution and 5-min sonication in an ultrasonic bath. The samples are then rinsed with deionized water. Dithionite-citric acid (10 ml) is added to each sample, and the solution is kept for 1 h in a water bath at 80 °C to remove any metal coatings. After being rinsed with deionized water, the sample undergoes oxidative cleaning with a basic potassium persulphate solution at 100 °C for 1 h to remove external organic N. The cleaned samples are rinsed in deionized water and dried overnight at 60 °C.

Conversion of foraminifera-bound N to nitrate. Foraminifera (3–6 mg per sample) are weighed into a previously combusted glass vial and dissolved in 4 N HCl (40–60 μl per sample). To convert the released organic N to nitrate, basic potassium persulphate oxidizing solution is added to each vial and to vials containing organic standards and procedural blanks, and the vials are then autoclaved for 1 h on a slow-vent setting (1.5 h including warm-up and cool-down times). To lower the N blank associated with the oxidizing solution, the potassium persulphate is recrystallized two to three times. At the time of processing, 1 g NaOH and 1 g potassium persulphate are dissolved in 100 ml of deionized water. Organic standards are used to constrain the δ^{15}N of the persulphate reagent blank. The two organic standards used here are mixtures of 6-aminocaproic acid and glycine. A minimum of 10 organic standards and 3–5 blanks are analysed per batch of samples, allowing for a correction for the persulphate blank. We used 1 ml of persulphate reagent for the blanks, oxidation standards and foraminifera samples.

Determination of N content. To determine sample N content, we measure nitrate concentration in the oxidation solutions after autoclaving. The nitrate analysis is done by reduction to nitric oxide using vanadium(III) followed by chemiluminescence detection[33]. The blank is also quantified in this way. The *G. ruber* and *G. sacculifer* samples have average N content of 3–4 μmol N per gram of sample, yielding nitrate concentrations in the oxidation solutions of 10–20 μM, whereas the blank concentration ranges between 0.3 and 0.7 μM.

Denitrifier method. A detailed explanation of the denitrifier method can be found in ref. 34. Before adding the foraminifera samples to the bacteria, the sample solution is acidified to pH 3–6. The denitrifier *Pseudomonas chlororaphis* was used for this work. Normally, 5 nmol samples are added to 1 ml of bacterial concentrate after the degassing. Oxidation standards, as well as replicate analyses of nitrate reference material IAEA-N3 (with δ^{15}N of 4.7‰) and a bacterial blank, are also measured. The IAEA-N3 standards are used to monitor the bacterial conversion and mass spectrometry, and the oxidation standards are used for the final correction of the data. If possible, samples are oxidized in duplicate, and all oxidized samples are analysed by the denitrifier method in duplicate at least. The reported error is the standard deviation (1σ) estimated from the means of separate oxidations of cleaned foraminiferal material.

Age model. We use the age model in refs 20,35. This age model is based on radiocarbon dating for the past 21.6 kyr. For the rest of the record, the age model is based on the alignment between the δ^{18}O record of *G. ruber* and the LR04 benthic stack reference curve[36].

Bulk sediment δ^{15}N analysis. The total N content of the sediment was analysed as N_2 using a Thermo Fisher Series 1112 elemental analyser coupled with a Thermo Fisher Delta V Plus mass spectrometer at ETH Zurich. Between 40 and 60 mg of sediment was analysed. In-house standards of atropine and peptone were measured in the same runs, and the final corrections were based on the peptone standard, which has been referenced to international reference materials. Standard deviations for both standards were <0.2‰.

X-ray fluorescence scanning. Sediment Zr/Al X-ray fluorescence (XRF) count ratios were obtained with an Avaatech XRF Core Scanner at MARUM, University of Bremen. Data were obtained at a resolution of 1 cm over an area of 1.2 cm^2 directly at the split-core surface of the archive half, with different settings for light elements such as Al (10 kV, 20 s and 150 mA) and heavy elements such as Zr (50 kV, 20 s and 800 mA). The core surface was covered with a 4-μm-thick SPEXCerti Prep Ultralene1 foil to avoid contamination of the XRF measurement unit. The core scanner includes a Canberra X-PIPS Silicon Drift Detector (SDD; Model SXD 15C-150-500) with 150-eV X-ray resolution, a Canberra Digital Spectrum Analyzer DAS 1000 and an Oxford Instruments 100W Neptune X-ray tube with rhodium target material. Raw data spectra were processed using the WIN AXIL package from Canberra Eurisys.

To bridge coring gaps and hiatuses, cores from all three parallel holes (A, B and C) were used, and a new composite depth was derived from the XRF data. Because cores from hole C had been frozen and re-thawed, we used this hole only where material from the other two holes was unavailable. The higher water content of Site 658C resulting from the different treatment affected the Al measurements, as is commonly observed. We therefore adjusted the Zr/Al ratios from Site 658C by regression to Zr/Al from Site 658B for a section with overlapping data (Supplementary Fig. 3).

The age model for the record from Site 658 was derived by transferring the published benthic δ^{18}O record[37] onto the new composite depth and aligning the record to the same data as contained in the LR04[36] benthic stack (Supplementary Fig. 3). For the past 15 kyr, the age model was further refined by aligning XRF Ca counts from Site 658A and Site 658B to percentage $CaCO_3$ data from radiocarbon-dated Site 658C[38,39], and for the period between 20 and 130 kyr ago, additional tie-points were derived by matching Zr/Al to the humidity index of core GeoB7920-2[40,41].

Because Zr from zircon minerals is dominantly present in the coarse silt fraction, whereas Al is most abundant in clay minerals, the Zr/Al ratio is interpreted to reflect grain size (Supplementary Fig. 3). Similarly, the Zr/Rb ratio has been shown to covary with grain size in this region[40,42], but the low signal-to-noise ratio of Rb in our XRF measurements led us to use Al instead. The dust deposited at Site 658 is mainly transported by the northeast trade winds, and its dominant grain type is coarse silt[43]. Increasing Zr/Al ratios at Site 658 should therefore reflect increasing aeolian transport of Saharan dust.

Map of excess phosphorus and wind velocities. The excess phosphorus map shown in Fig. 1 uses World Ocean Atlas data[44] and the software Ocean Data View[45]. Winds were plotted using the IRI Climate and Society Map Room (http://iridl.ldeo.columbia.edu/maproom).

33. Braman, R. S. & Hendrix, S. A. Nanogram nitrite and nitrate determination in environmental and biological materials by vanadium(III) reduction with chemiluminescence detection. *Anal. Chem.* **61,** 2715–2718 (1989).
34. Sigman, D. M. *et al.* A bacterial method for the nitrogen isotopic analysis of nitrate in seawater and freshwater. *Anal. Chem.* **73,** 4145–4153 (2001).
35. Schmidt, D. W., Spero, H. J. & Lea, D. W. Links between salinity variation in the Caribbean and North Atlantic thermohaline circulation. *Nature* **428,** 160–163 (2004).
36. Lisiecki, L. E. & Raymo, M. E. A. Pliocene-Pleistocene stack of 57 globally distributed benthic δ^{18}O records. *Paleoceanography* **20,** PA1003 (2005).
37. Sarnthein, M. & Tiedemann, R. Toward a high-resolution stable isotope stratigraphy of the last 3.4 million years: Sites 658 and 659 off Northwest Africa. *Proc. ODP Sci. Res.* **108,** 167–661 (1989).
38. deMenocal, P. *et al.* Abrupt onset and termination of the African Humid Period: rapid climate responses to gradual insolation forcing. *Quat. Sci. Rev.* **19,** 347–361 (2000).
39. Adkins, J., deMenocal, P. & Eshel, G. The "African humid period" and the record of marine upwelling from excess ^{230}Th in Ocean Drilling Program Hole 658C. *Paleoceanography* **21,** PA4203 (2006).
40. Tjallingii, R. *Application and Quality of X-Ray Fluorescence Core Scanning in Reconstructing Late Pleistocene NW African Continental Margin Sedimentation Patterns and Paleoclimate Variations* 65–84. PhD thesis, Univ. Bremen (2006).
41. Tjallingii, R, *et al.* Coherent high- and low-latitude control of the northwest African hydrological balance. *Nature Geosci.* **1,** 670–675 (2008).
42. Matthewson, A. P., Shimmield, G. B., Kroon, D. & Fallick, A. E. A 300-kyr high-resolution aridity record of the North-African continent. *Paleoceanography* **10,** 677–692 (1995).
43. Holz, C., Stuut, J. B. W. & Henrich, R. Terrigenous sedimentation processes along the continental margin off NW Africa: implications from grain-size analysis of seabed sediments. *Sedimentology* **51,** 1145–1154 (2004).
44. Garcia, H. E. *et al. World Ocean Atlas 2009* Vol. 4, 398 (Government Printing Office, 2010).
45. Schlitzer, R. Ocean Data View. http://odv.awi.de (2012).